Original Research Article

Wind Turbine Systematic Wake to Wake Analysis: Quantification of Turbulence and Statistical Analysis for Optimal Wind Farm Design

ABSTRACT

Through this work, we have analyzed wake to wake interactions between horizontal axis wind turbines located in line to each other. We have analyzed wake interactions based on hot wire anemometric data and statistical correlations using a model wind farm fabricated inside a wind tunnel. The results of these measurements show that a high level of turbulent kinetic energy is generated at the region of intersection between rotor and stator wakes. Numerical models of wake interactions of wind turbines under varying turbulent inflow conditions using the actuator line technique and EllipSys3D Navier-Stokes solver were carried out and showed good agreement with field measurements of wake deficit and turbulence intensity for inline turbines.

Keywords: Renewable energy, wind turbine wakes, statistical correlations, hot wire anemometry

UNDER PEER REVIEW

1. INTRODUCTION

Wind energy has become a major focus in the push to provide renewable energy to a growing world population. Wind turbine energy production influences due to operating conditions and related research is important for the design of maximum efficiency wind farms. Wakes have been shown to produce adverse effects on the performance of wind turbines. It is therefore important to understand the complex development of wakes from turbines and how wake-wake interactions influence other turbines [1].

Wakes can be divided into two distinct regions, the near and far wake respectively, based on rotor proximity. In the near wake region, which spans from 2 to 4 rotor diameters behind a turbine, fluid dynamics are dominated by axial forces stemming from mechanical power extraction Tip vortices generated by the blades decay within the near wake and the velocity regains a Gaussian profile [2]. Far wake regions begin after the tip vortices have decayed entirely and can last as long as 15 rotor diameters. Far wake persistence is greater than typical row spacing within a wind farm which makes understanding the interactions in this region key to total wind farm performance. Within the far wake, turbulence decays with regard to the incoming velocity deficit and turbulence intensity [2]. Turbulence intensity determines the bow induced rotor loads and systematic wake impacts on downstream turbines of the wind farm [2].

Medici and Alferdson [3] highlighted changes in the wake model stemming from oncoming free stream turbulence and the importance of structure dynamics resulting from these streams. The low frequency vortex shedding (Von Karman vortex street) was found to be present in all of the velocity components, indicating three-dimensional behavior. The shedding frequency corresponds to bluff body behavior. Medici and Alferdson [3] used two-point cross-correlation of the velocity signals, an important technique in wake-wake interaction investigation. Investigations into the behavior of wake-wake interactions include both experimental and numerical studies. Experimental investigation of wake-wake interactions in a turbomachine have been conducted with PIV measurements [4]. The results of these measurements show that a high level of turbulent kinetic energy is generated at the region of intersection between rotor and stator wakes. These regions of high turbulent kinetic energy, dubbed turbulent ”hot spots,” are observed to have twice the amount of turbulent kinetic energy when compared to the turbine wake before the wake-wake interaction. Numerical models of wake interactions of wind turbines under varying turbulent inflow conditions using the actuator line technique and EllipSys3D Navier-Stokes solver were carried out and show good agreement with field measurements of wake deficit and turbulence intensity for two inline turbines [4]. Other numerical investigations have looked into numerous wake interaction numerical modeling techniques for optimal design of wind farms [5]. Blind studies were conducted where various groups around the world made attempts to model wake development in wind farms [6]. These models were compared to experimental data. Wake interactions are stated as being problematic for turbulence modelers. Further numerical models for wake-wake turbine interactions have been constructed showing good comparison to experimental data [7]. Numerical models have also been compared to simple engineering models used in the design of wind farms [6].

2. EXPERIEMENTAL SETUP

2.1 Wind Tunnel

The experiments were conducted in a wind tunnel equipped with an active grid at the University of Newfoundland as shown in Figure 1. The tunnel is a closed-circuit design with a cross section of 0.8 m x 1.0 m and a test section 5 m in length. The active grid is constructed of 7 horizontal and 9 vertical rotating axis flaps, with each axis individually controlled by stepper motors. The model turbines had a rotor diameter of D = 0.2 m, a nacelle diameter of d = 0.028 m, a cylindrical tower with diameter dt = 0.015 m, and a hub height of h = 0.24 m. A Cartesian turbine array was constructed of four such turbines. Turbines were spaced at distances of 2D from one another in the crossflow direction and 4.5D in the streamwise direction. Turbines were selectively added or removed to examine the full combination of wakes downstream of the array. Three variations of turbine location were considered as depicted in Fig. 2.

UNDER PEER REVIEW

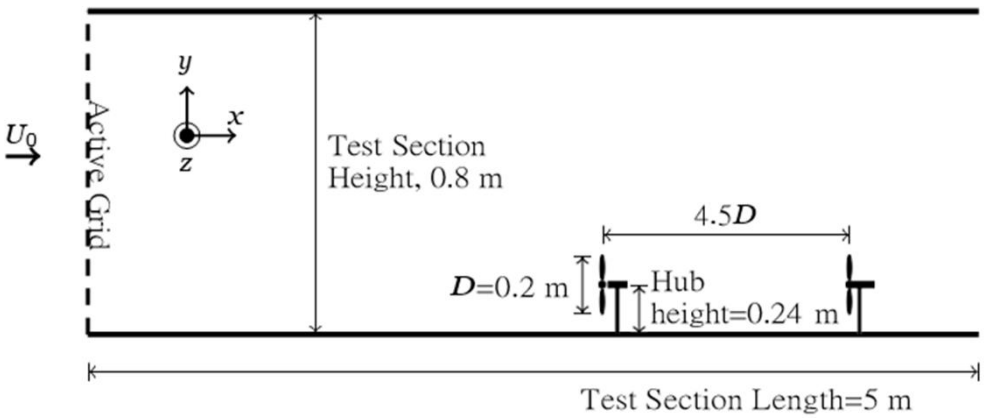

Figure 1: Tunnel Setup

2.2 Inflow Conditions

Experiments were conducted under two different inflow conditions. The first was a low turbulence inflow condition with an average turbulence intensity of 4.0%. The second scenario was the high turbulence inflow condition with an average turbulence intensity of 10.0%. Low turbulence inflow was created by a fixed passive grid where the active grid axes were held stationary and parallel to the flow direction (passive inflow). Turbulence was realized by imposing the motion of the active grid axes (active inflow). The Weitemeyer protocol was used [8] to create a statistically reproducible turbulent inflow by controlling the motion of the active grid axis. The angle of attack, α, was changed at a rate of 2 Hz with Gaussian distributions possessing a mean of zero and a standard deviation of 25◦. Changes in the blockage of the active grid were compensated for by introducing a phase shift of 90◦ between the axes of the active grid so the incoming velocity converged to 5.9 m/s. The flow conditions were then measured at the location of the wind turbines, X = 0D, to characterize the flow. For the active and passive grid cases, hot-wire measurements were taken for 2 and 1.5 mins, respectively, at the locations where the turbines were placed.

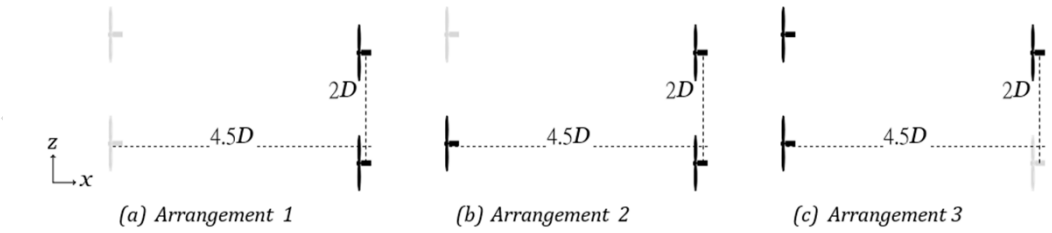

Figure 2: Turbine arrangements: (a) two turbines next to each other (b) one upstream with two downstream and (c) two upstream with one downstream.

2.3 Hot Wire Measurements

Hub height velocity measurements were recorded with a single line of hot-wires consisting of eleven 1-D hot-wires (Fischer Scientific 13245257) of 1 mm length. The hot wires were operated using a pair of Fischer Scientific multichannel CTAf54N80 devices with a low-pass filter set at 10 kHz. Data acquisition was conducted using an 18-bit A/D converter (NI 6281) at a sampling frequency of 20 kHz.

The hot wires were calibrated with the active grid in an open configuration at low turbulence. The hot- wires were positioned at the end of the closed test section to ensure turbulence generated by grids was well mixed before reaching hot wires as to not influence calibration. Two Prandtl tubes connected to pressure sensors were used to measure the mean velocity over a time period of 120s to achieve converged means for pressure and hot-wire sensors. The velocity range for the calibration was 1.0 m/s - 9.0 m/s in steps of 1 m/s. A second calibration following the same procedure was performed in order to confirm matching with the first calibration to exclude drift hot-wires. Calibrations were carried out every four hours and at the end of the experiments to ensure hot-wire calibrations remained satisfactory.

The hot-wires were arranged at three locations downstream of the turbine array. The total span of the measurements was 5D with hot-wires positioned at distances of x/D = 1, x/D = 3, and x/D = 5 as shown in Fig. 3. Hot-wires spacing in the span-wise direction was 0.075 m and was reduced in the center to 0.05 m to provide additional resolution in the crossflow direction.

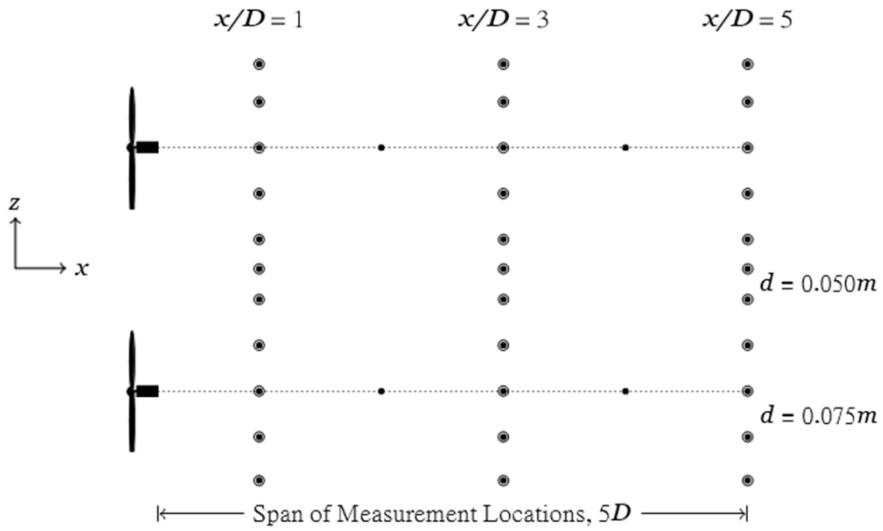

Figure 3: Hub height hot-wire positions behind the turbine array. Note the reduced spacing for the hot-wires in the center of each array.

3. THEORY

As turbulence intensity is one of the major factors contributing to turbulent wake formation and interaction, the first consideration is this key parameter. Turbulence intensity is expressed as the ratio of the root mean squared velocity, U_{rms}, in the direction of mean flow to the mean velocity, $\overline{U}$:

$$I_u = \frac{U_{rms}}{\overline{U}} \qquad (1)$$

where U_{rms}, is found from the fluctuating component of the velocity, as described by the Reynolds decom- position:

$$U_{rms} = \sqrt{u'^2} \quad (2)$$

$$u' = U - \bar{U} \quad (3)$$

The velocity deficit can be found by first considering the turbulent kinetic energy equation from the scalar product of the mean velocity with the RANS. This equation may be simplified by recalling the far wake region is sufficiently far downstream of the turbine blades and so viscous effects are negligible [2]. Thus, the simplified turbulent kinetic energy equation can be written as follows:

$$U_j \frac{\partial \frac{1}{2} U_i^2}{\partial x_j} = -\frac{1}{\rho} U_i \frac{\partial P}{\partial x_i} + \overline{u_\iota u_j} \frac{\partial U_i}{\partial x_i} - \frac{\partial \overline{u_i u_j} U_i}{\partial x_j} - F_x \quad (4)$$

Where, $\frac{1}{\rho} U_i \frac{\partial P}{\partial x_i}$ express the pressure gradient, $\overline{u_\iota u_j} \frac{\partial U_i}{\partial x_i}$ is the turbulent kinetic energy production by Reynold's shear stresses, $\frac{\partial \overline{u_i u_j} U_i}{\partial x_j}$ is the turbulent kinetic energy flux from high to low scales, and F_x represents the energy extracted by a turbine. In the far wake region, turbulence production and energy flux are the terms of interest. Thus, pressure gradients and turbine energy extraction are near wake phenomena. They are responsible for defining the initial far wake conditions, whereas far wake regions are defined by turbulent energy production from high to low scales.

3.1 Boundary Layer Characteristics

Because turbines remove energy from the flow, they act in a similar manner to drag with regard to momentum and energy [2]. Therefore, the equations for displacement, momentum, and energy thickness may be applied across the range from $-\infty$ to ∞. Displacement thickness, δ_1, of the flow field in the near wake region is computed as:

$$\delta_1 = \int_{-\infty}^{\infty} (1 - \frac{\overline{u(z)}}{U_\alpha}) dz \quad (5)$$

where u(z) is the mean velocity at the near wake region at a distance of z from the turbine axis. From the same approach, momentum thickness, δ_2, and energy thickness, δ_3, can be written as,

$$\delta_2 = \int_{-\infty}^{\infty} \frac{\overline{u(z)}}{U_\alpha} (1 - \frac{\overline{u(z)}}{U_\alpha}) dz \quad (6)$$

The shape factor, H, is defined as the ratio of the displacement thickness to momentum thickness as:

$$\delta_3 = \int_{-\infty}^{\infty} \frac{\overline{u(z)}}{U_\alpha} (1 - \frac{\overline{u(z)^2}}{U_\alpha}) dz \quad (7)$$

UNDER PEER REVIEW

These equations may be computed numerically from velocity measurements in known positions along the z-axis.

$$H = \frac{\delta_1}{\delta_2} \qquad (8)$$

3.2 Two Point Statistics

The point-wise correlation between two distinct points in a stationary random process is,

$$R_i = < u_i(x,t)u_i(x+r,t) > \quad (9)$$

where the velocities at the two points are separated by the distance r and R_i is the i^{th} correlation coefficient between two velocity vectors. Final two-point correlation is based on,

$$C_i = \frac{R_i}{\sigma(u\prime(x))\sigma(u\prime(x+r))} \qquad (10)$$

Where σ is the standard deviation of the considering fluctuating velocity components of the points and σ_i is the i^{th} value of the correlation. Two-point correlation coefficient ranges from the minimum value of -1 to the maximum of 1. A high positive value signifies a strong positive correlation in flow between two points while a highly negative value indicates a strong negative correlation. A value of zero represents no correlation between two points.

4. RESULTS AND DISCUSSION

4.1 Analysis of the Downstream Flow Fields

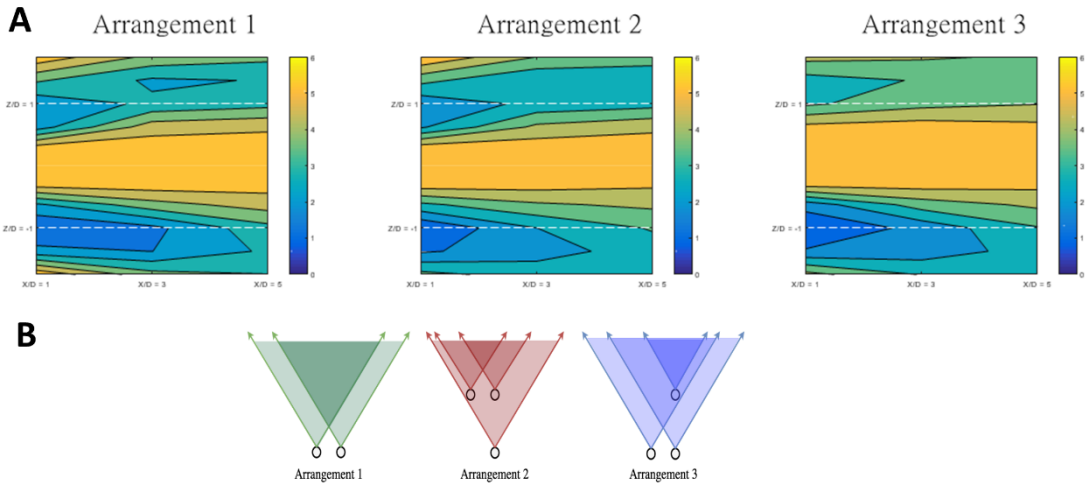

Figure 4: (A). Average velocity fields behind each turbine arrangement. Upstream turbine locations are denoted with dashed lines. (B). Wake interaction zones corresponding to each turbine arrangement

PEER REVIEW

Figure 4 shows the average velocity fields of each turbine arrangement with passive inflow. The influence of the asymmetric turbine arrangement is the most dominant in Arrangement 3. This asymmetry correlates with the physical wake asymmetry shown in Fig. 5. Figure 6 shows differences in mean flow velocity measured at hub height for passive and active inflow conditions for the three different turbine con- figurations normalized by the free stream velocity. Velocity measurements are averaged across the hot wires from hub to hub of the wind turbines.

For the comparison of mean velocities of arrangements 1 and 2, the difference in velocities was smallest at x/D = 1, where the deviation is near zero, with increased deviation at x/D = 3 followed by the largest deviation at x/D = 5. This is observed for both the active and passive inflow cases. The active inflow was shown to have a greater deviation in velocities compared to the passive case. Comparison of arrangements 1 and 3 shows the opposite trend in deviation of velocities where differences were largest at x/D = 1, then decreased at x/D = 3, and were smallest at x/D = 5. The active inflow case was shown to have a smaller overall deviation than the passive case. Comparison of arrangements 2 and 3 shows a similar trend in deviation of velocities where differences were largest at x/D = 1, followed by a decrease in deviation at x/D = 3. However, a slight increase in deviation is observed at x/D = 5. In this comparison, though, the active and passive inflow cases showed near identical deviations in velocities. The largest overall deviation in average velocities is seen in the comparison of configurations 1 and 3 and in comparison, of configurations 2 and 3 with the smallest relative deviation seen in configurations 1 and 2. Differences in mean velocities show that arrangements 1 and 2 are the most similar while arrangements 1 and 3, and 2 and 3 are most dissimilar. This is observed for both the active and passive cases. From the arrangement of the turbines, it is observed that case 1 and 2 are similar and only differ in that an extra turbine is placed upstream from the two downstream turbines directly in front of the bottom turbine for arrangement 2. Arrangement 3 has a third turbine placed behind the two upstream turbines with the third turbine placed directly behind the top turbine. Differences in mean velocities show that wakes upstream interacting with turbines downstream do not influence the flow as much. In other words, a singular disturbance upstream does not influence the downstream region as much as a singular downstream turbine does. For arrangement 2, the two downstream turbines are symmetrically mixing an asymmetric flow, while in arrangement 3 the downstream turbine is asymmetrically mixing a symmetrically mixed flow. It is therefore reasonable to think that case 2 should be more similar to case 1, since in case 1 there are only two turbines symmetrically mixing the free stream flow. This reasoning is supported by Fig. 6.

Figure 7 shows comparisons of the average turbulence intensity normalized by the free stream turbulence intensity for passive and active inflow conditions at the three measurement locations for the three different turbine configurations. Measurements are averaged across the hot-wires from hub to hub of the wind turbines. For the comparison of arrangements 1 and 2 and the comparison of arrangements 1 and 3, similar trends are observed. For the passive case, the largest deviation in mean turbulence intensity is observed at x/D = 1, with decreased deviations at x/D = 3, and the smallest deviations at x/D = 5. In the active case, the largest deviations are seen at x/D = 1 with the smallest at x/D = 3, and an increase by x/D = 5.

UNDER PEER REVIEW

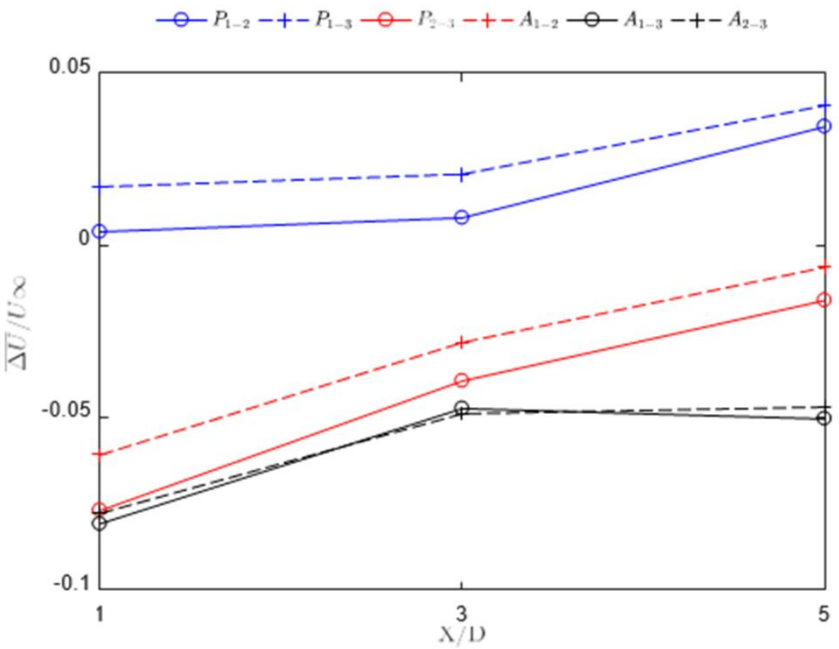

Figure 6: Differences between mean velocities normalized by the free stream velocity for the various turbine arrangements at the three downstream locations. Each color corresponds to a turbine arrangement while solid lines represent passive inflows and dashed show active inflow conditions

For comparison of arrangements 2 and 3, the deviations in mean turbulence intensities were largest at x/D = 1 for both active and passive inflow cases. Differences in turbulence intensity increased with downstream distance and are shown to be a maximum at x/D = 5. Differences in mean turbulence intensity are always smaller across all positions and arrangement always smaller across all positions and arrangement comparisons for the active inflow condition with the exception of comparisons of arrangements 1 and 2 and arrangements 1 and 3 at x/D = 5 where the active inflow condition increased the deviation in turbulence intensity compared to the passive case.

The attenuation of the mean turbulence intensity difference across arrangements in the active case is believed to be a result of the more homogeneous state of the flow for the active inflow case compared to the passive inflow case. In the passive case, the turbulence intensity in the free stream is 6% smaller than that of the active case. The disturbance to the flow field is more pronounced in the passive case due to a smaller turbulence intensity in the free stream. In other words, disruption to the flow is more pronounced in the passive case. Furthermore, the downstream development of the turbulence in- tensity is more pronounced in the passive case when compared to the active case. This again is due to the flow being in a more homogeneous state in the active case, where disturbances due to the turbines are less pronounced, relatively. For all comparisons in the active case, the difference in turbulence in- tensity goes to zero at x/D = 3. It is at this point, x/D = 3, that the flow in the active case has re- gained its inflow characteristics. For the passive case, however, turbulence intensity does not go to zero until x/D = 5 and perhaps even further down-stream in the case of comparisons of case 2 and 3. Furthermore, the differences in mean turbulence intensity were larger for the passive case. This is again due to the disturbances playing a larger role in the passive inflow case due to the turbulence intensity being 6% lower

UNDER PEER REVIEW

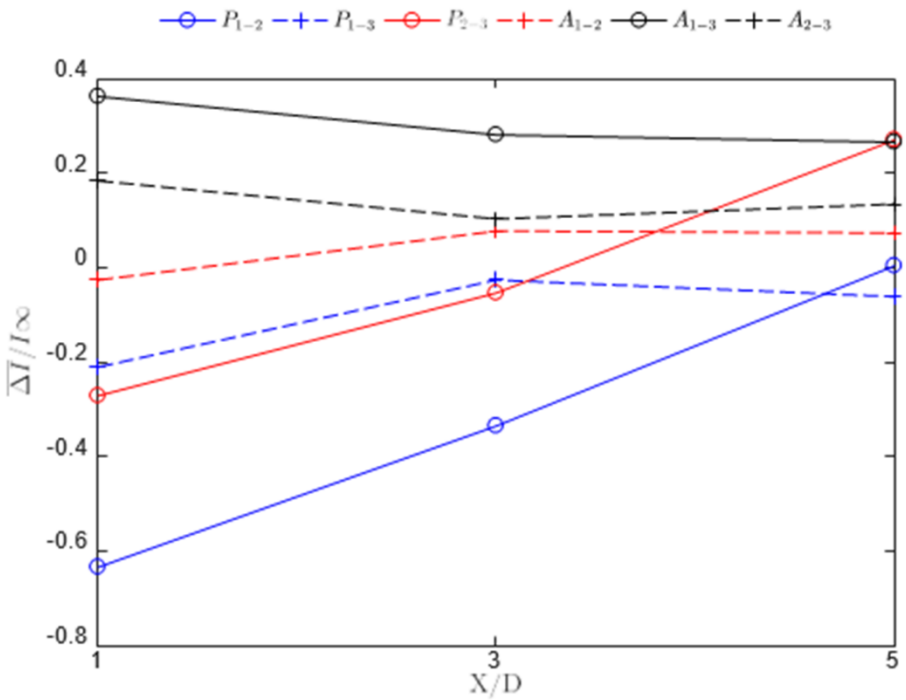

Figure 7: Differences between average turbulence intensity normalized by the free stream turbulence intensity for the various turbine arrangements at the three downstream locations. The color scheme from Figure 6 has been maintained for consistency.

The displacement, momentum, and energy layers are similar between arrangements with the active inflow condition resulting in 0.01 m larger thicknesses than the passive inflow scenario. Displacement decreases with downstream distance as the flow regains a parabolic velocity profile within the wake region. Displacement thickness is greater than energy thickness which is greater than momentum thickness independent of arrangement. Both momentum and energy thickness increase for much longer downstream distances than displacement and are still increasing at x/D = 5.

UNDER PEER REVIEW

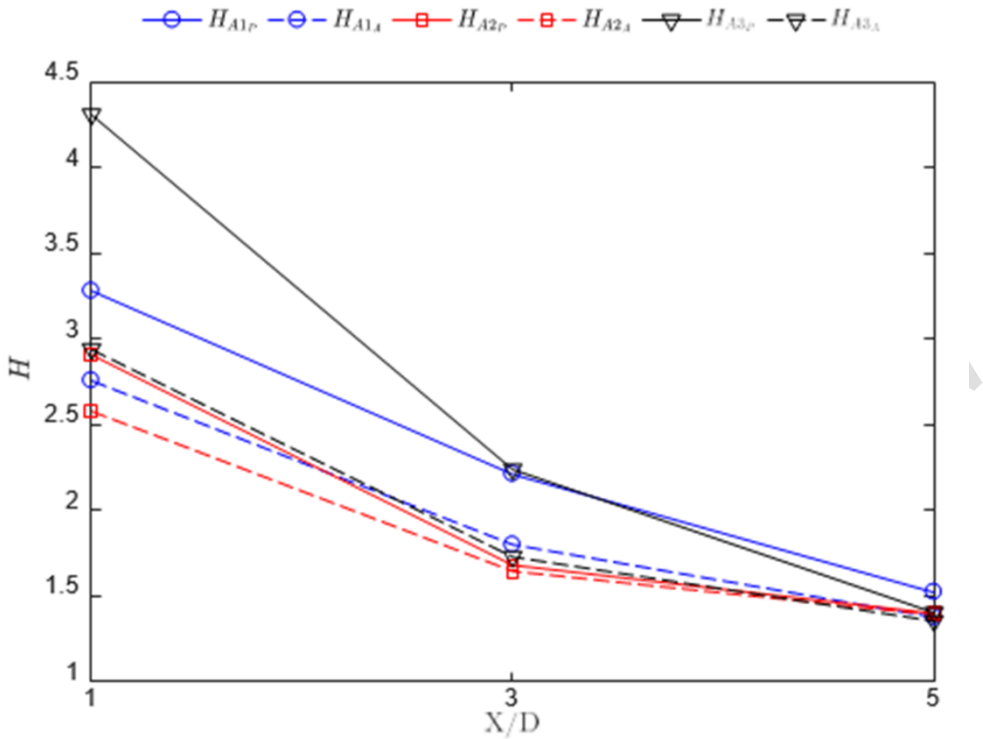

Figure 8: Shape factor across all arrangements. The color scheme from Figure 6 has been maintained for consistency.

Energy thickness variation along the downstream is greatly influenced by the symmetry of arrangements since at arrangement 1, increase of energy thickness is comparably lower than other two cases implying the difficulty in regaining its original state. As concluding remarks, this phenomenon demonstrates the greater persistence of wakes in the far-wake region as compared to the near-wake region. Although the flow can regain a parabolic velocity profile within a few diameters, the turbulent energy produced by the rotating blades must traverse the energy cascade and in doing so create momentum and energy layers which persist far beyond the initial disturbance. The interactions be- tween wakes further enhances turbulent energy pro- duction, increasing the downstream distance before the flow fully recovers it's momentum.

4.3 Two Point Statistical Analysis

Two-point correlations were considered for each arrangement at each hot wire location behind the array. An example of which is depicted in Fig. 10. It was observed that close to the turbines, the center of the flow is highly correlated with itself in the first arrangement for the passive inflow condition and in all arrangements for the active inflow conditions. Similarly, to the differences in turbulence intensity described previously, symmetry does not appear to affect alter wake interactions as dramatically for active inflows. For passive inflow conditions, the extreme spanwise locations are correlated across all arrangements as the fluid closest to the boundary layer regains the free stream velocity.

The possible explanation for this is due to asymmetric effects from arrangements 2 and 3, flow field loses its uniformity due to induced turbulence so loses the correlation. It is also

UNDER PEER

observable that the strength of the correlation for the far ends decreases with distance downstream as the wake edges expand beyond the furthest spanwise measurement locations. Arrangements 2 and 3 possess a slight correlation in the center similar to arrangement 1. Both of these arrangements are more homogeneously mixed than arrangement 1 leading to lower correlations overall. The possible explanation for this occurrence is that arrangement 2 has an asymmetric turbine placement to front from the back row which expose the back row turbine from a single wake. However, in arrangement 3 back turbine is exposed to nearly a symmetric wake structure from front two turbines.

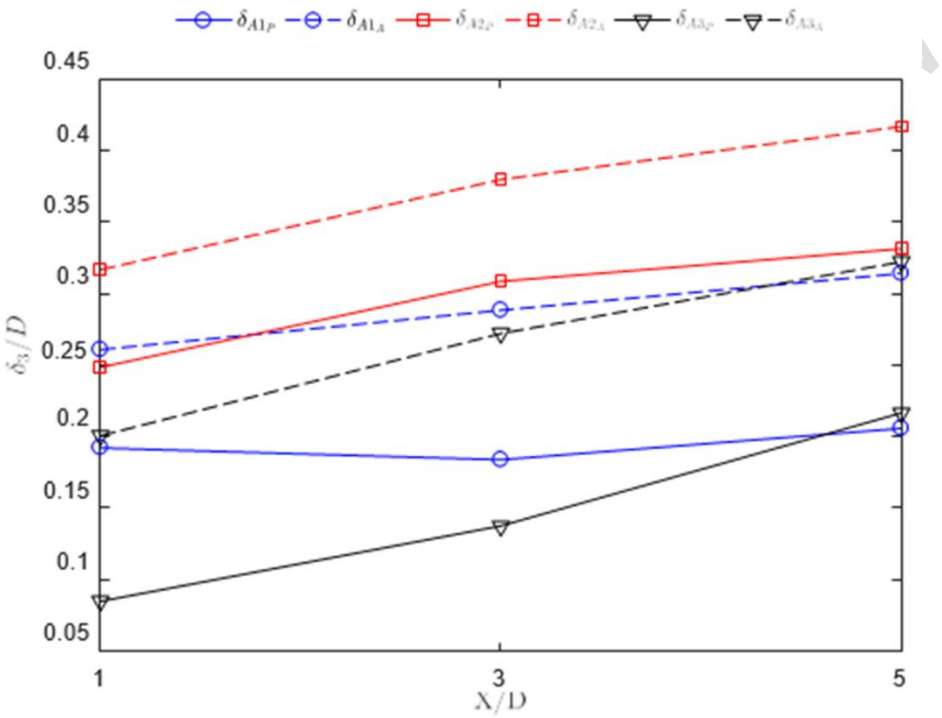

Figure 9: Energy thickness across all arrangements. The color scheme from Figure 6 has been maintained for consistency.

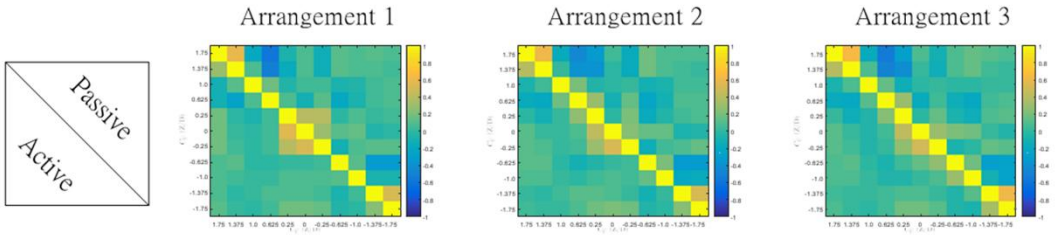

Figure 10: Two-point correlation matrix at x/D = 3 for each arrangement. The upper-right corner contains correlation coefficients for passive inflow conditions and the lower-left contains the active inflow coefficients. The main diagonal is composed of self-correlations between hot wires.

4.4 Spectral Analysis

The hub-height velocities at Z/D = -1, 0, 1 and X/D = 1, 3, 5 were investigated through spectral analysis for all arrangements. These locations were selected to further examine the flow directly behind the turbines and in the center of the mixing region. In order to quantify each scenario, the spectra of the passive and active grid inflow conditions were evaluated at X/D = 0. As shown in Fig. 11, the passive inflow exhibits a peak at low wave numbers near 3 corresponding to structures of approximately 0.3 m in size. The peak is followed by an energy cascade following Kolmogorov's 5 line suggesting the incoming flow is dominated by the large structures formed by the passive grid. The active grid flow is dominated by larger structures of 1 m in size as evidenced by a peak at the lowest wave numbers. The passive inflow possessed less turbulent energy at each location than the active inflow.

Directly behind the turbines, the active and passive inflows collapse to similar energy levels which increase with distance downstream. As shown in Fig. 11, this occurs regardless of turbine arrangement. Within the mixing area, the spectrum at z/D = 0 exhibits a large peak in the passive inflow scenario and plateau in the active inflow scenario. The peaks and plateaus align at an approximate wave number of 8, corresponding to structures of 0.1 m, independent of turbine arrangement. The magnitude of the peak in the passive scenario is larger than the inflow conditions indicating an injection of energy into the turbulent flow at this scale. This energy injection is of similar size to the radius of the model turbine, so it is reasonable to assume the turbulence imparted by the rotating turbine blades interacts in the mixing region which directly contributes to turbulent energy production in the wake region.

UNDER PEER REVIEW

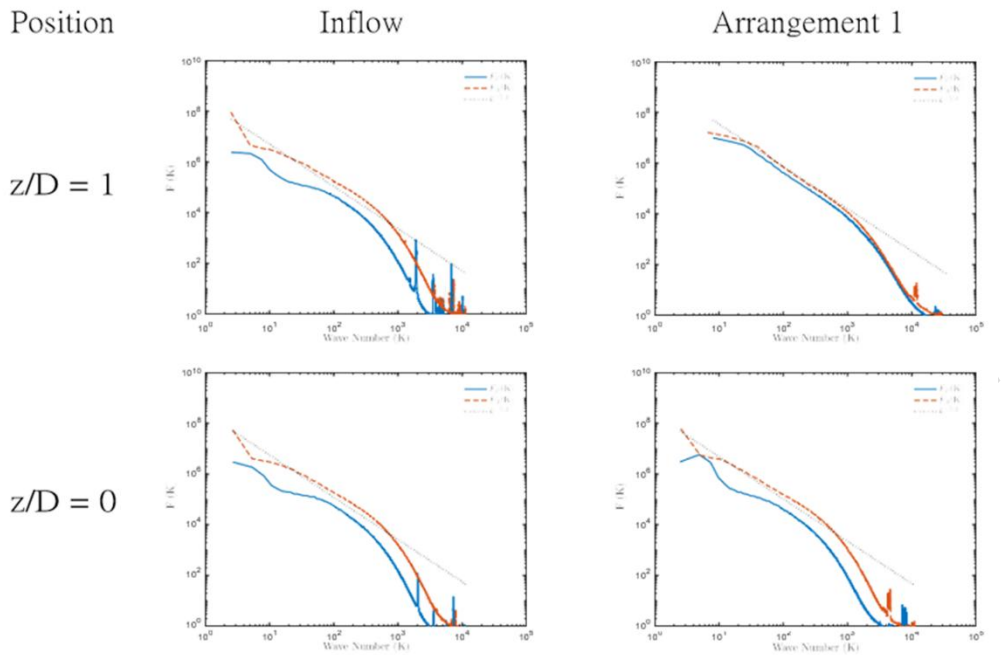

Figure 11: Selected spectra at x/D = 3. Solid blue curves indicate passive inflow conditions while red dashed curves show the active scenario. The theoretical decay is provided in each figure for reference.

4. CONCLUSION

Normalized mean velocity differences showed that the various turbine arrays disrupted the flow in entirely different manners. The position of the third turbine in arrangements 2 and 3 made a significant difference in the development of average flow velocity where arrangement 3 was observed to be dissimilar from the other two arrangements. This is due to asymmetric disruption of the flow in arrangement 3 due to the placement of the third turbine behind the two upstream turbines, causing an asymmetric disturbance to the flow. Investigations into mean turbulence intensity differences between arrangements suggest that turbulence intensity of the inflow is an important factor for the variation in the mean turbulence intensity between arrangements. Less difference in mean turbulence intensity is seen in the active inflow condition compared to the passive inflow condition. This is due to the homogeneous mixing associated with the active inflow condition where the inflow is more turbulent. Further, for all turbine arrangement comparisons in the active case, differences in mean turbulence intensity seem to converge to near zero at x/D = 3. This behavior is not seen in the passive inflow case until x/D = 5, and in some cases, further downfield. Two-point correlations and spectral analysis support the assertion that the point at which wakes merge produces high levels turbulent production. This production greatly enhances the persistence of the far wake region as evidenced by the development of the momentum and energy thicknesses. The intensity of the turbulence at this junction and subsequent increase in wake longevity is dependent on the upstream layout of the turbines. Asymmetric upstream flows were found to produce the greatest increase in turbulence intensity leading to high turbulent production and enhanced wake longevity.

COMPETING INTERESTS DISCLAIMER:

Authors have declared that no competing interests exist. The products used for this research are commonly and predominantly use products in our area of research and country. There is absolutely no conflict of interest between the authors and producers of the products because we do not intend to use these products as an avenue for any litigation but for the advancement of knowledge. Also, the research was not funded by the producing company rather it was funded by personal efforts of the authors.

REFERENCES

[1] G. M. Joselin Herbert, S. Iniyan, E. Sreevalsan, and S. Rajapandian, "A review of wind energy technologies," *Renewable and Sustainable Energy Reviews*, vol. 11, no. 6, pp. 1117–1145, Aug. 2007, doi: 10.1016/j.rser.2005.08.004.

[2] L. J. Vermeer, J. N. Sørensen, and A. Crespo, "Wind turbine wake aerodynamics," *Progress in Aerospace Sciences*, vol. 39, no. 6–7, pp. 467–510, Aug. 2003, doi: 10.1016/S0376-0421(03)00078-2.

[3] V. Mendoza and A. Goude, "Improving farm efficiency of interacting vertical-axis wind turbines through wake deflection using pitched struts," *Wind Energy*, vol. 22, no. 4, pp. 538–546, Apr. 2019, doi: 10.1002/we.2305.

[4] I. Dobrev and F. Massouh, "CFD and PIV investigation of unsteady flow through Savonius wind turbine," *Energy Procedia*, vol. 6, pp. 711–720, 2011, doi: 10.1016/j.egypro.2011.05.081.

[5] J. Kuo, D. Rehman, D. A. Romero, and C. H. Amon, "A novel wake model for wind farm design on complex terrains," *Journal of Wind Engineering and Industrial Aerodynamics*, vol. 174, pp. 94–102, Mar. 2018, doi: 10.1016/j.jweia.2017.12.016.

[6] J. Castro Mora, J. M. Calero Barón, J. M. Riquelme Santos, and M. Burgos Payán, "An evolutive algorithm for wind farm optimal design," *Neurocomputing*, vol. 70, no. 16–18, pp. 2651–2658, Oct. 2007, doi: 10.1016/j.neucom.2006.05.017.

[7] H. Sun, X. Gao, and H. Yang, "A review of full-scale wind-field measurements of the wind-turbine wake effect and a measurement of the wake-interaction effect," *Renewable and Sustainable Energy Reviews*, vol. 132, p. 110042, Oct. 2020, doi: 10.1016/j.rser.2020.110042.

[8] S. Weitemeyer, D. Kleinhans, T. Vogt, and C. Agert, "Integration of Renewable Energy Sources in future power systems: The role of storage," *Renewable Energy*, vol. 75, pp. 14–20, Mar. 2015, doi: 10.1016/j.renene.2014.09.028.

UNDER PEER REVIEW